Intrinsically Stretchable and Healable Semiconducting Polymer for Skin-Inspired Wearable Organic Transistors

Jin Young Oh[1‡], Simon Rondeau-Gagné[1‡], Yu-Cheng Chiu[1,2‡], Alex Chortos[1], Franziska Lissel[1], Ging-Ji Nathan Wang[1], Bob C. Schroeder[1], Tadanori Kurosawa[1], Jeffrey Lopez[1], Jie Xu[1], Chenxin Zhu[3], Xiaodan Gu[1,4], Won-Gyu Bae[1], Yeongin Kim[3], Lihua Jin[1], Jong Won Chung[1,5] Jeffrey B.-H. Tok[1] and Zhenan Bao[1]*

[1] Department of Chemical Engineering, Stanford University, Stanford, CA 94305-5025, USA

[2] Department of Chemical Engineering and Materials Science, Yuan Ze University, Taoyuan 32003, Taiwan

[3] Department of Electrical Engineering, Stanford University, Stanford, CA 94305-5025, USA

[4] Stanford Synchrotron Radiation Lightsource SLAC National Accelerator Laboratory, Menlo Park, CA 94025, USA

[5] Samsung Advanced Institute of Technology, Yeongtong-gu , Suwon-si, Gyeonggi-do 443-803 , Korea

‡ *These authors have equal contribution to this work*

Developing a molecular design paradigm for conjugated polymers applicable to intrinsically stretchable semiconductors is crucial toward the next generation of wearable electronics.[1,2] Current molecular design rules for high charge carrier mobility semiconducting polymers are unable to render the fabricated devices simultaneously stretchable and mechanically robust.[3] Herein, we present a new design concept to address the above challenge, while maintaining excellent electronic performance. This concept involves introducing chemical moieties to promote dynamic non-covalent crosslinking of the conjugated polymers. These non-covalent covalent crosslinking moieties are able to undergo an energy dissipation mechanism through breakage of bonds when strain is applied, while retaining its high charge transport ability. As a result, our polymer is able to recover its high mobility performance (>1 cm^2/Vs) even after 100 cycles at 100% applied strain. Furthermore, we observed that the polymer can be efficiently repaired and/or healed with a simple heat and solvent treatment. These improved mechanical properties of our fabricated stretchable semiconductor enabled us to fabricate highly stretchable and high performance wearable organic transistors. This material design concept should illuminate and advance the pathways for future development of fully stretchable and healable skin-inspired wearable electronics.

Thin-film field-effect transistors (TFTs) are fundamental elements of stretchable electronic devices.[4] To realize stretchable TFTs, all of its components need to be also stretchable. Whereas recent significant progress has been made towards stretchable conductors,[5-8] the realization of stretchable semiconductors has been focused mainly on strain-accommodating engineering either via wavy structures or blending of nanofibrils or nanowires into elastomers.[9-11] However, these approaches are based on materials that are not intrinsically stretchable, which will invariably limit their durability, application scope and, importantly, increase the complexity of device fabrication.

Another approach relies on intrinsically stretchable semiconductors, so that they can easily be fabricated using standard processing methods.[12] It was reported that the molecular stretchability was enhanced when these conjugated polymers, containing modified side-chains and segmented backbone, are infused with more flexible molecular building blocks.[13,14] Nonetheless, these polymers reported to date (which are mainly conjugated polymers), do not simultaneously possess both high mobility and high stretchability.

Incorporating polar substituents in organic semiconductors has been widely investigated in recent organic electronics research.[15] Not only the morphologies of the polymer will be influenced by the introduced polar substituents, these functionalities often also confer dynamic behaviors to the polymer chains. Incorporation of dynamic non-covalent crosslinking between the flexible polymer chains is an important strategy to achieve high stretchability and self-healing properties.[16,17] The dynamic bonds can be easily broken to allow energy dissipation upon strain, thus enabling the system to be more tolerant to strain and mechanical stimuli. However, they can be reformed to recover the initial mechanical property or self-heal. Among the different types of dynamic bonds, hydrogen bonding is particularly suited for skin-inspired electronics due to their spontaneous formation and healing ability.[18-21]

Herein, we present a new material design concept for highly stretchable and high charge carrier mobility conjugated polymers through incorporation of H-bonding moieties to partially break the conjugation to lower elastic modulus and simultaneously to enable intermolecular dynamic bonding. These new semiconducting polymers exhibit high stretchability and, moreover, healing ability upon mechanical damage. Organic thin-film field-effect transistors (OTFTs) fabricated from these materials exhibited mobility as high as 1.3 cm^2/Vs and high on/off current ratio ($> 10^6$). The mobility remained as high as 1.12 cm^2/Vs at 100% strain along perpendicular direction to strain. The mobility of damaged devices can be recovered, from 0.024 to 1.13 cm^2/Vs after a healing treatment. To the best of our knowledge, this work reports the first demonstration of an intrinsically stretchable and healable semiconducting polymer using in OTFTs working at high strain conditions. Finally, we successfully fabricated a skin-inspired stretchable organic transistor operating under extensive human motions.

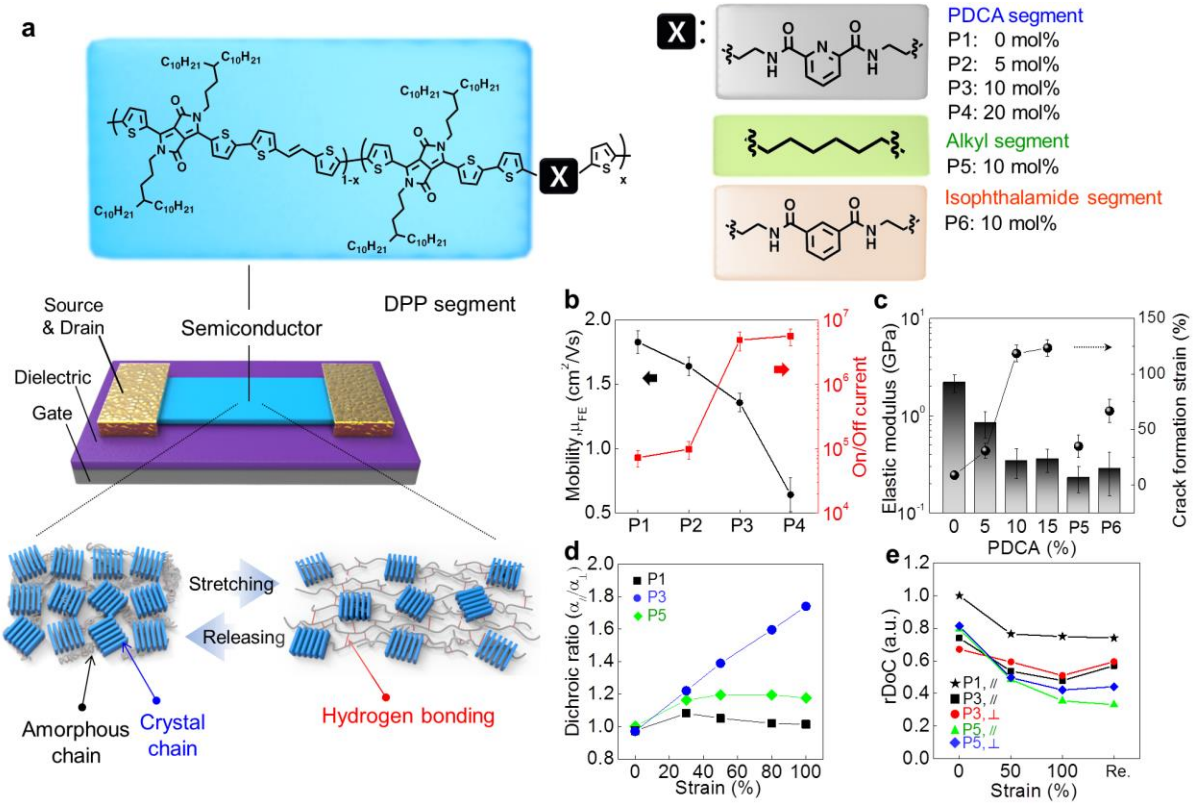

Figure 1 | Design of stretchable and healable semiconducting polymer OTFTs and their performance characterizations. a) Chemical structures of polymers **P1** to **P6** and general mechanism for enhancement of stretchability in conjugated polymers via dynamic bonding. The stretchable semiconducting polymers are based on 3,6-di(thiophen-2-yl)-2,5-dihydropyrrolo[3,4-*c*]pyrrole-1,4-dione (DPP) repeating units and non-conjugated 2,6-pyridine dicarboxamide (PDCA) moieties introduced directly in the polymer backbone as hydrogen bonding units. To qualitatively evaluate the stretching properties of the polymers, thin films are supported on PDMS substrates and stretched to different strain ratios (0 to 100% strain); b) Field-effect mobility and on/off current ratios of **P1** to **P4** as measured by conventional OTFTs (Source and drain electrode: Au, 40 mn, dielectric layer: SiO_2, 300 nm, gate electrode: highly doped silicon substrate); c) Influence of the hydrogen bonding moiety amount on elastic modulus and crack formation strain; d) Dichroic ratios of **P1**, **P3** and **P5** under various strain. $\alpha_{//}$ and $\alpha_{\perp}$ are absorption intensity measured with the polarization direction of light parallel and perpendicular to the stretching direction; e) Influence of the strain ratio on the relative degree of crystallinity (rDoC) extracted from peak (200) for both "parallel" and "perpendicular" directions of **P1**, **P3** and **P5.** Due to large crack formation, rDoC of **P1** perpendicular to strain direction was not measured.

2,6-pyridine dicarboxamide (PDCA) was chosen to introduce hydrogen bonding within the flexible polymer backbone since this unit contains two amide groups possessing moderate H-bonding strength, allowing the formation of a polymer network without drastically increasing the tensile modulus of the material.[22,23] Previous literatures have indicated that introducing a small fraction of non-conjugated units to the polymer backbone did not significantly degrade the charge

transport mobility.[24] Here, we proceed to introduce alkyl spacers to enhance the flexibility of the dynamic moieties. Semiconducting polymers incorporating different ratios of non-conjugated PDCA moiety were thus synthesized (**P1** to **P4**, structures shown in Figure 1a). To confirm the presence of hydrogen bonds, both X-ray crystallography and NMR experiments (Extended Data Figures 1 & 2 and Figure S1, S2 and S7) were utilized to ascertain H-bond formations in PDCA-containing model compounds.

Initial evaluation of the electrical properties was performed with OTFT devices (Figure 1b). For devices fabricated with **P2** and **P3**, the measured mobilities were both >1 cm^2/Vs. Even with **P4** (containing 20 mol% of non-conjugated monomers), its field-effect mobility remained as high as 0.58 cm^2/Vs (Figure S8). To further understand the contributions from disruption of conjugation and incorporation of H-bonding on the mechanical properties of the polymers, we next measured the elastic modulus of the polymers (Figures 1c & S9). All the polymers with PDCA moieties exhibited a lower elastic modulus in comparison to the polymer without H-bonding (**P1**). Even though intermolecular H-bonding essentially crosslinked the polymers and should hence increase the elastic modulus of the polymer film,[25] it appears that disruption of conjugation, i.e. reducing the rigidity of the conjugated polymer backbone, have a more significant effect on the elastic modulus of the polymer semiconductor film. We attributed the lowering in the measured elastic modulus to the change in film morphology, such as the increase in the amorphous fraction in the polymer film or decrease in relative crystallinity (rDoC) (Fig. 1e), and also a slight reduction of the average size of crystallites (Extended Data Figure 3c), as characterized by grazing incidence X-ray diffraction (GIXD) analysis (Figure S10). Lower elastic modulus asserts a lower stress on the material under the same strain. Hence, this allows the material to be stretched to higher strains before cracks begin to form.

To gain further insight into the molecular level changes during stretching, the degree of polymer chain alignment under strain was measured using polarized UV-vis spectroscopy and quantified using dichroic ratios (Figures 1d, S12). The dichroic ratio of **P1** initially increased slightly with strain due to strain-induced chain alignment, but soon decreased to ~1 caused by chain relaxation due to crack formation upon increasing the strain from 30% to 100%. This observation indicates that **P1** is not very stretchable and, indeed, we observed that cracks began to form even at low strains (5~10 %), which were further confirmed by both optical microscopy and atomic force microscopy (AFM). On the other hand, the dichroic ratio of **P3** increased linearly to 1.8, as strain

increased from 30-100%. This observation is consistent with our microscopic observations that no microscale cracks were formed for **P3**, even with strain as high as 100%, hence polymer chain alignment by strain can be continuously achieved. (Figures S13, S14 and Extended Data Figure 3)

Relative degree of crystallinity (rDoC) analysis was used next to examine the molecular-level morphology of the polymers under strain (Figures 1e & S15-16). The rDoC of **P1** decreased with strain from 0-50%, and plateaued from 50% onwards. This observation, combined with AFM studies, indicate that the tensile strain applied on the thin film was initially released through breakage of the crystalline regions until crack formation. In contrast, rDoC of **P3** decreased steadily upon 0-100% applied strain. Upon releasing strain, we observed that the rDoC only partially recovered, indicating some of its crystalline domains may be permanently altered/broken apart due to the applied strain. This result, combined with the observed steady increase in dichroic ratio previously, suggest that **P3** has multiple mechanisms for energy dissipation during strain: (i) stretching and realignment of polymer chains in amorphous regions, (ii) breaking of some of the crystalline domains, and (iii) breakage of H-bonding.

Energy dissipation mechanism through H-bond breakages has previously been demonstrated.[18] We confirmed this benefit from incorporating H-bonding sites as strain releasing moieties by comparison with a reference polymer, **P5,** containing 10 mol% of non-conjugated alkyl spacers, i.e. no PDCA moieties, on its polymer backbone (Figure 1a). Despite having a lower elastic modulus than **P3**, the reference polymer **P5** can only achieve a maximum strain of 30% before cracks formation, a value much lower than that of **P3** maximum strain (110%). Furthermore, the measured maximum dichroic ratio for **P5** was found to be only ~1.16 at 30% strain, consistent with strain value for onset of crack formation. In addition, the relative crystallinity of **P5** was measured to be lower than **P1,** indicating an increase in the fraction of amorphous regions has occurred within the polymer thin film, similar to **P2-P4**. However, when 100% strain was applied on the film, the rDoC decreased drastically from 0.80 to 0.35, indicating that the tensile energy in **P5** film is dissipated primarily through the breaking of crystallites. Compared to **P1-P4**, the huge difference in the strain behavior of **P5** (lacking PDCA moieties) confirmed the important contribution of the dynamic non-covalent H-bond forming moieties as strain-releasing elements (Figure S17). We also proceed to perform the synthesis of a new semiconducting polymer in which the pyridine moiety was replaced by a simple benzene ring (**P6**, Figure 1a). Stretchability tests using roll-transfer printing were subsequently performed with **P6** and our obtained results are

summarized in Figure 1c and S14. **P6** was observed to possess enhanced stretchability compared to polymer **P1** and **P5**, which indicates the importance of the intermolecular hydrogen bonding for enhanced mechanical properties. However, as compared to polymers **P2**, **P3** and **P4** (all containing a pyridine moiety), the stretchability of all these polymer was reduced. Therefore, our finding underscores the importance of the pyridine moiety in enhancing the polymer's overall mechanical properties. This was accomplished as the pyridine moiety is able to introduce additional intramolecular hydrogen bonds to modify the final morphology of the polymer chains.

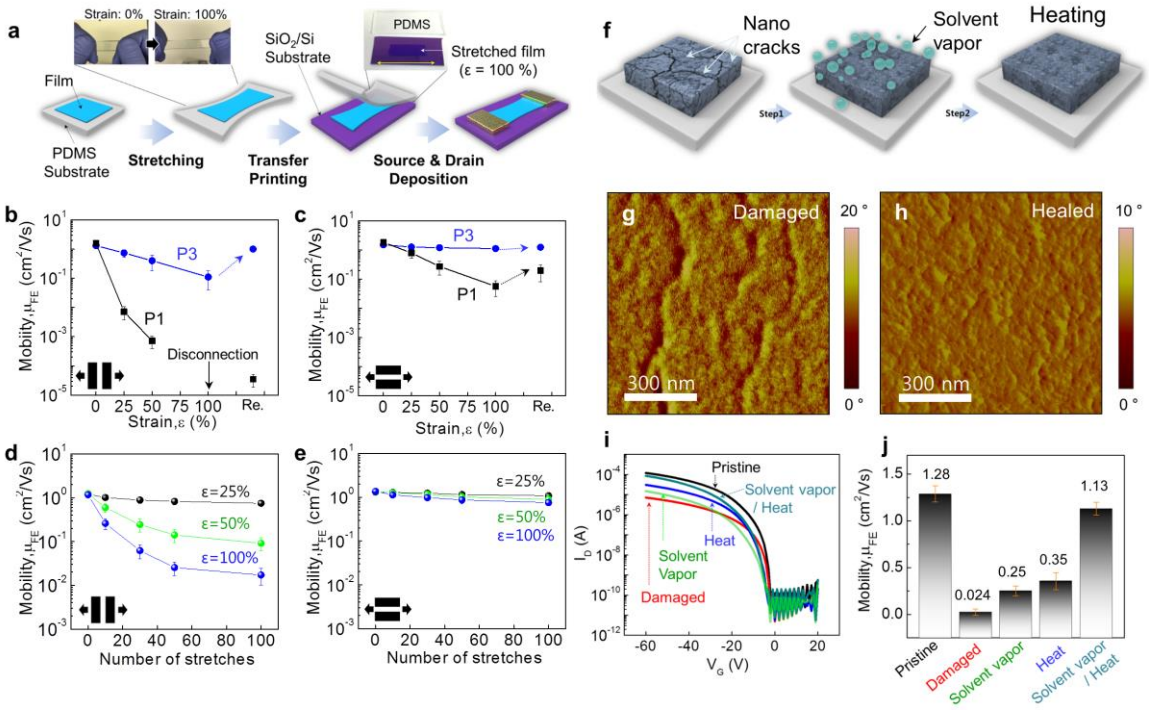

Figure 2 | Charge transport of semiconducting polymers under applied strain and their healing properties. a) Fabrication process for OTFTs with stretched polymer thin films; b) field-effect mobility as a function of various strains along the strain direction and c) perpendicular to strain direction; d) field-effect mobility versus number of stretching cycle performed along the strain direction and e) perpendicular to strain direction; f) Representation of the treatments used for healing the conjugated polymer films; g) AFM phase image for damaged and h) healed film of **P3**; i) Transfer curves, and j) Field-effect mobility of damaged and healed **P3** OTFTs .

To evaluate the charge transport behavior of our fabricated stretchable semiconducting polymers, OTFTs were fabricated and characterized (Figure 2a). Upon applying strains up to 100%, we observed that the average field-effect mobility of the **P3** device only decreased slightly, from 1.32 cm^2/Vs to 0.11 cm^2/Vs, along the direction of applied strain. Furthermore, the mobility was observed to recover to 1.00 cm^2/Vs upon releasing the applied strain. When the strain is applied in a perpendicular direction, the mobility of **P3** device is maintained, i.e. >1 cm^2/Vs, up to 100%

strain and even after release. In contrast, the mobility of **P1** device degraded significantly even at 25% applied strain, and was totally non-functional at 100% strain. Unlike **P3**, the mobility of **P1** devices are unable to recover upon stress release. Besides single stretching event, we also performed rigorous repeated stretching cycle tests on the **P3** devices at various strains (Figures 2d-e). After stretching the device for 100 cycles in between 0-25% strain, in specific, even after 100 cycles up to 100% strain, only a 26% decrease in mobility was observed; while only a 19% decrease in mobility was observed for 100 cycles up to 25% strain (Figure S18), the mobility along the stretching direction was decreased by ~40 % (i.e., 1.2 to 0.74 cm^2/Vs) and was further reduced to 0.017 cm^2/Vs when subjected to 100% strain. However, when the strain is along the perpendicular direction, the device showed higher durability and robustness.

In addition to intrinsic stretchability, the healing ability enabled by the dynamic bonding represents another major advantage of the polymer design. Although the self-healing abilities of non-conjugated polymer networks crosslinked with H-bonding sites have been reported,[26] self-healing ability has not been investigated for conjugated polymer. To facilitate efficient healing for damaged **P3** films, post treatments via heat and/or solvent annealing are required to promote polymer chains movement (Figure 2f). When applied independently, both thermal and solvent annealing significantly reduced the size and density of the nanocracks. However, the field-effect mobility was observed to only be slightly recovered (Figures 2g-j & S19). On the other hand, solvent annealing applied in conjunction with thermal annealing allowed the most efficient healing of the polymer films. In specific, we observed a complete disappearance of the nanocracks within the damaged films, and more importantly, an almost complete recovery of the average field-effect mobility to 1.13 cm^2/Vs (Figures 2i-j & S19). Additionally, the dependence of dichroic ratio on strain completely recovered to a similar level as a pristine undamaged film, indicating the healed film has most probably returned to its original film morphology. In comparison, our various applied healing conditions did not improve the damaged **P1** and **P5** films (Figures S20-24 and Extended Data Figure 4). To the best of our knowledge, this is the first demonstration of complete healing (albeit non-autonomous) of a high field-effect mobility conjugated polymer after mechanical damages.

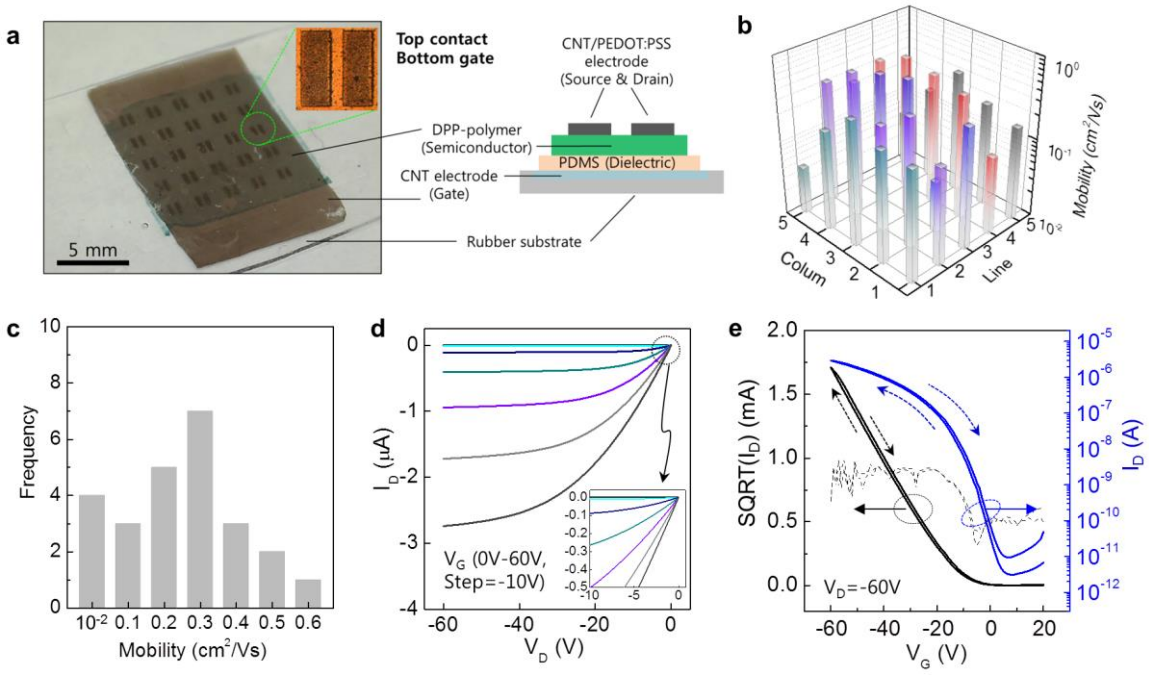

Figure 3| **Stretchable transistors characterization.** a) Photograph and architecture of a fully stretchable 5x5 organic transistor array fabricated via our developed stretchable conjugated polymers; b,c) mapping statistical distribution of the field-effect mobility in our transistor array; d,e) output and transfer curves of fully stretchable organic transistor 5x5 array.

Equipped with our newly developed high mobility and high stretchability polymer semiconductor, we proceed to fabricate fully stretchable OTFTs (5x5 arrays; Figures 3a, S25 & Extended Data Figure 5). Our obtained device yield is 100%, along with good switching performance (Figures 3b-e). Furthermore, most of the devices exhibited field-effect mobilities in the range of ~10^{-1} cm^2/Vs with >10^5 on/off current ratio (Figures S25). In specific, the highest value obtained for the mobility is 0.6 cm^2/Vs, while the average mobility was 0.28 cm^2/Vs. In general, we observed that the fully stretchable OTFTs all exhibited lower mobilities compared to OTFTs as fabricated on rigid OTS-treated Si/SiO_2 substrates. We attributed this observation to the lower applied electric field with a thicker layer of dielectric on the stretchable OTFTs devices (Figure S26). The stretchable devices showed little hysteresis and low gate-leakage currents. These measured performance parameters represent the best among the current reported stretchable organic semiconductors and fully stretchable OTFTs (Tables S3 & S4). [27-30]

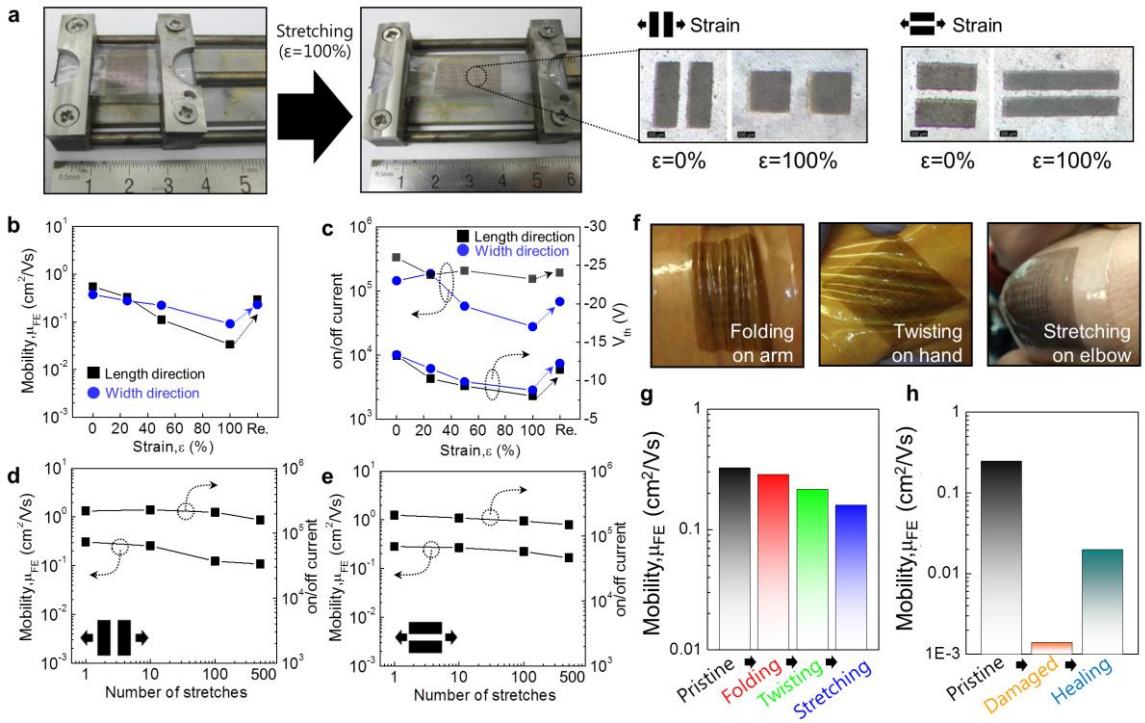

Figure 4 | Stretchable transistor as skin-inspired wearable device. a) *In-situ* stretching images of stretchable OTFT from 0% to 100 % strain (scale bar = 300 μm); b) mobility, c) on/off current ratio, and threshold voltage of stretchable transistor during a stretching cycle. Mobility and on/off ratio of OTFTs for 500 times stretching cycle at 25% strain; d) channel length and e) width directions; f) Photographs of folded, twisted, and stretched OTFTs on human skin; and g) OTFT mobilities after various extreme human motions; h) Mobilities of mechanically damaged OTFTs before and after healing process.

To verify the stretchability of our organic transistors, we investigated their electrical performance by subjecting them to various strenuous mechanical strain conditions. The transistors showed a slow linear decrease in mobility when being strained up to 100%. After releasing the strain, the mobility was observed to recover to close to its initial values (Figures 4b & S27). The same trend was also observed for the on/off current ratios. These trends are qualitatively similar to the trend observed with only the polymer semiconductor being stretched. Considering that most practical applications only require accommodation in between 20-30% applied strain, stretching durability tests at 25% strain and 500 cycles were thus performed for our fabricated stretchable transistors (Figures 4d-e). We observed that both the field-effect mobility and on/off current ratio of our transistors did not suffer any significant decrease in performance. Furthermore, we proceed to mount our fabricated devices on human limbs to test for tolerance under various common motions, such as folding of arm, twisting of hand, and stretching on elbow. We observed that our device is able to maintain its mobility at >0.1 cm^2/Vs (Figure S28) under all these examinations. Finally,

the healing ability of the polymer semiconductor can again be observed using our developed heating and solvent annealing process (Figures 4h & S29).

Conclusions

We describe herein a rational new design concept for highly robust, stretchable, healable and high mobility semiconducting polymer to enable the next-generation skin-inspired wearable electronic. This was accomplished by incorporating non-conjugated 2,6-pyridine dicarboxamide (PDCA) moieties to partially disrupt the polymer conjugation such as to reduce crystallinity, to reduce elastic modulus and, importantly, to enable dynamic non-covalent inter- and intra-molecular crosslinking of the conjugated semiconducting polymers. Collectively, these factors contributed to the simultaneous enhancement in stretchability and mechanical robustness of a healable polymer semiconductor. We have also successfully demonstrated a highly performing organic transistor 5x5 arrays fabricated solely with intrinsically stretchable electronic materials. In summary, our described molecular design concept should advance the further development of mechanically robust stretchable polymer electronic materials towards skin-inspired wearable electronics.

Acknowledgement

This work was supported by Samsung Electronics and the Air Force Office of Scientific Research (grant no. FA9550-15-1-O10B). Simon Rondeau-Gagné acknowledges the Fonds de Recherche Québécois, Nature et Technologie (FRQNT) for a postdoctoral fellowship. Yu-Cheng Chiu acknowledges the Ministry of Science and Technology, Taiwan, for partially financial support (project 104-2923-E-002-003-MY3). Bob C. Schroeder acknowledges the National Research Fund of Luxembourg for financial support (project 6932623). Jeffrey Lopez acknowledges support from the National Science Foundation Graduate Research Fellowship Program under Grant No. DGE-114747.

Author Contribution

J. Y. O., S. R.-G., Y.-C. C. and Z. B. conceived and designed the experiments. S. R.-G. and Z.B. designed the monomers and polymers. S.R.-G., B.C.S., T.K. and F.L. synthesized and characterized the monomers and polymers. J. Y. O designed the device experiments and evaluated the stretchability of materials and devices. Y.-C. C. and J. Y. O. fabricated and optimized the OFETs on solid substrates. J. Y. O. designed and fabricated the fully stretchable OTFTs. J. Y. O., A. C., and C. Z. optimized the fully stretchable devices. J. Y. O. designed and performed the healing experiments. J. Y. O., G.-J. N. W., J. X., L. G., J. L., J. W. C., J. L. and Y. K. analyzed the optical and mechanical properties of the polymer film. Y.C.C. performed the GIXD experiments and analysis. Y.-C. C., X. G., S. R.-G., J. Y. O. and Z. B. proposed the new mechanism concept. J. Y. O. and W.G.B. designed and drew the 3D computer graphics.

J. Y. O., S. R.-G., Y.-C. C., J. B.-H. T. and Z. B. co-wrote the paper. All authors discussed the results and commented on the manuscript.

Methods

All details of materials synthesis and structural characterizations can be found in the Supplementary Information.

Materials Synthesis and Characterization

Synthesis of DPP-based conjugated polymers containing non-conjugated PDCA units in the backbone was carried out via Stille polymerization using different ratios of PDCA-containing monomers (Scheme S1 and S2). Branched alkyl chains were installed on the DPP monomer in order to increase solubility and π-π stacking. We also selected (E)-2-(2-(thiophenyl-2-yl)vinyl)thiophene (TVT) as co-monomer. The non-conjugated monomer was reacted with the brominated DPP monomer and the distannylated thienovinylthiophene (TVT) under Stille polymerization conditions to afford **P1** to **P4**. Polymers were purified by precipitation in methanol followed by Soxhlet extraction using methanol, acetone, hexanes and chloroform. Polymers presented a good solubility in different solvents such as chloroform and chlorobenzene. Increasing the non-conjugated moiety content within the backbone also improved the solubility in polar solvents such as THF and DMF. Synthetic procedure for precursors, monomers and polymers are detailed in Supplementary Information. Molecular weight, polydispersity index, monomers and polymers characterization are all detailed in Supplementary Information.

.

Thin-films Characterizations

Morphology of polymer films was measured by optical microscopy and AFM. Molecular stretchability of polymer film was investigated by polarized UV-vis spectroscopy. Elastic modulus of thin-films was measured by buckling method (Figure S24). Grazing incidence X-ray diffraction (GIXRD) was conducted at beamline 11-3 of the Stanford Synchrotron Radiation Lightsource. The incidence angle was 0.12 and the X-ray wavelength was 0.9758 Å, corresponding to a beam energy of 12.7 keV. All of GIXRD images were collected in reflection mode with a two-dimensional area detector and the sample in a helium atmosphere. All of samples were spin-cast on SiO_2/Si or OTS-treated SiO_2/Si substrates at a spin rate of 1000 rpm for 60s from prepared polymer solutions in chlorobenzene (5 mg/mL). Stretching and relaxing rates of the polymer thin films were performed at 0.65 mm/sec.

Device Fabrications

Conventional organic transistors: Semiconducting polymer layer (35 nm) was spin coated on OTS-treated SiO_2/Si substrate in glove box and was thermally annealed at 150 °C for 10 minute. Source and drain electrode (Au, 40nm) was thermally evaporated under 5.0×10^6 Torr.

Skin-inspired organic transistor: Carbon nanotube (CNT, 100 nm) film as gate electronic was transferred on SEBS elastomer. PDMS layer (1.8 μm) was then transferred on CNT/SEBS substrate. Semiconducting polymer layer (35 nm) was then transferred on the PDMS dielectric layer. Finally, PEDOT:PSS (30 nm)/CNT (70 nm) bilayer as source

and drain electrode is spray coated on the semiconducting layer. The transferring method for the device fabrication was specifically depicted in Extended Data Figure 5.

Healing process

Solvent vapor treatment: the damaged sample is exposed for $CHCl_3$ vapor in a closed jar for 10 min. at 40 °C. Heat treatment: the sample is thermally annealed on 150 °C hotplate for 30 min. Solvent vapor / heat treatment: A sequential combination of $CHCl_3$ vapor annealing (10 min. at 40°C) and thermal annealing (30 min. on hotplate at 150°C).

References

1. Chortos, A. & Bao, Z. Skin-inspired electronic devices. *Mat. Today* 17, 321–6038 (2014).
2. Wagner, S. & Bauer, S. Materials for stretchable electronics. *MRS Bulletin* 37, 207-213 (2012).
3. Savagatrup, S. *et al.* Molecularly stretchable electronics. *Chem. Mater.* 26, 3028–3041 (2014).
4. Hammock, M. L. *et al.* 25th Anniversary article: the evolution of electronic skin (E-skin): A brief history, design, consideration, and recent progress. *Adv.Mater.* 25, 5997–6038 (2013).
5. Yao, S. & Zhu, Y. Nanomaterial-enabled stretchable conductors: Strategies, materials, and devices. *Adv.Mater.* 27, 1480–1511 (2015).
6. Benight, S. J., Wang, C., Tok, J. B. H. & Bao, Z. Stretchable and self-healing polymers and devices for electronic skin. *Prog. Polym. Sci.* 38, 1961–1977 (2013).
7. Oh, J. Y. *et al.* Conducting polymer dough for deformable electronics. *Adv. Mater.* DOI: 10.1002/adma.201502947 (2015).
8. Sekitani, T. *et al.* Stretchable active-matrix organic light-emitting diode display using printable elastic conductors. *Nat. Mater.* 8, 494 - 499 (2009).
9. Kaltenbrunner, M. *et al.* Ultrathin and lightweight organic solar cells with high flexibility. *Nat. Comm.* 3, 770 (2012).
10. Khang, D.-Y., Jiang, H., Huang, Y. & Rogers, J. A. A stretchable form of single-crystal silicon for high performance electronics on rubber substrates. *Science.* 311, 208–212 (2006).
11. Shin, M. *et al.* Polythiophene nanofibril bundles surface-embedded in elastomer: A route to a highly stretchable active channel layer. *Adv. Mater.* 27, 1255–1261 (2015).
12. O'Connor, B. *et al.* Anisotropic structure and charge transport in highly strain-aligned regioregular poly(3-hexylthiophene). *Adv. Funct. Mater.* 21, 3697–3705 (2011).
13. Müller, C. *et al.* Tough, Semiconducting polyethylene-poly(3-hexylthiophene) diblock copolymers. *Adv. Funct. Mater.* 17, 2674–2679 (2007).
14. Printz, A. D. *et al.* Increased elasticity of a low-bandgap conjugated copolymer by random segmentation for mechanically robust solar cells. *RSC Adv.* 4, 13635 (2014).
15. Gsänger, M. *et al.* Organic semiconductors based on dyes and color pigments. *Adv. Mater.* 28, 3615-2645 (2016).
16. Yang, Y. & Urban, M. W. Self-healing polymeric materials. *Chem. Soc. Rev.* 42, 7446–67 (2013).

17. Black Ramirez, A. L. *et al.* Mechanochemical strengthening of a synthetic polymer in response to typically destructive shear forces. *Nat. Chem.* 5, 757-761 (2013).
18. Chen, Y., Kushner, A. M., Williams, G. a. & Guan, Z. Multiphase design of autonomic self-healing thermoplastic elastomers. *Nat. Chem.* 4**,** 467–472 (2012).
19. Sun, J. Y. *et al.* Highly stretchable and tough hydrogels. *Nature* 489, 133-136 (2012)
20. Cordier, P., Tournilhac, F., Soulié-Ziakovic, C. & Leibler, L. Self-healing and thermoreversible rubber from supramolecular assembly. *Nature* 451**,** 977–980 (2008).
21. Yuk, H. *et al*. Tough bonding of hydrogels to diverse non-porous surfaces. *Nat. Mater.* 15, 190–196 (2016)
22. Ray, M., Ghosh, D., Shirin, Z. & Mukherjee, R. Highly stabilized low-spin iron(III) and cobalt(III) complexes of a tridentate bis-amide ligand 2,6-bis(N-phenylcarbamoyl)pyridine. Novel nonmacrocyclic tetraamido-N coordination and two unusually short metal-pyridine bonds. *Inorg. Chem.* 36**,** 3568–3572 (1997).
23. Marlin, D. S., Olmstead, M. M. & Mascharak, P. K. Extended structures controlled by intramolecular and intermolecular hydrogen bonding: A case study with pyridine-2,6-dicarboxamide, 1,3-benzenedicarboxamide and N,N'-dimethyl-2,6-pyridinedicarboxamide. *J. Mol. Struct.* 554, 211–223 (2000).
24. Zhao, Y. *et al.* Conjugation-break spacers in semiconducting polymers: impact on polymer processability and charge transport properties. *Macromolecules,* 48, 2048–2053 (2015).
25. Langley, N. R. & Polmante, K. Relation of elastic modulus to crosslink and entanglement concentrations in rubber networks. *J. Polym. Sci., Part B: Polym. Phys.* 12, 1023–1034 (1974).
26. Herbst, F., Döhler, D., Michael, P. & Binder, W. H. Self-healing polymers via supramolecular forces. *Macromol. Rapid Commun.* 34, 203–220 (2013)
27. Song, E. *et al.* Stretchable and transparent organic semiconducting thin film with conjugated polymer nanowires embedded in an elastomeric matrix. *Adv. Electron. Mater.* 2, 1500250 (2016).
28. Wu, H.-C. *et al.* A rapid and facile soft contact lamination method: Evaluation of polymer semiconductors for stretchable transistors. *Chem. Mater.* 26, 4544–4551 (2014).
29. Chortos, A. *et al.* Highly stretchable transistor using microcracked organic semiconductor. *Adv. Mater.* 26, 4253–4259 (2014).
30. Kaltenbrunner, M. *et al.* An ultra-lightweight design for imperceptible plastic electronics. *Nature* 499, 458-463 (2013).

a

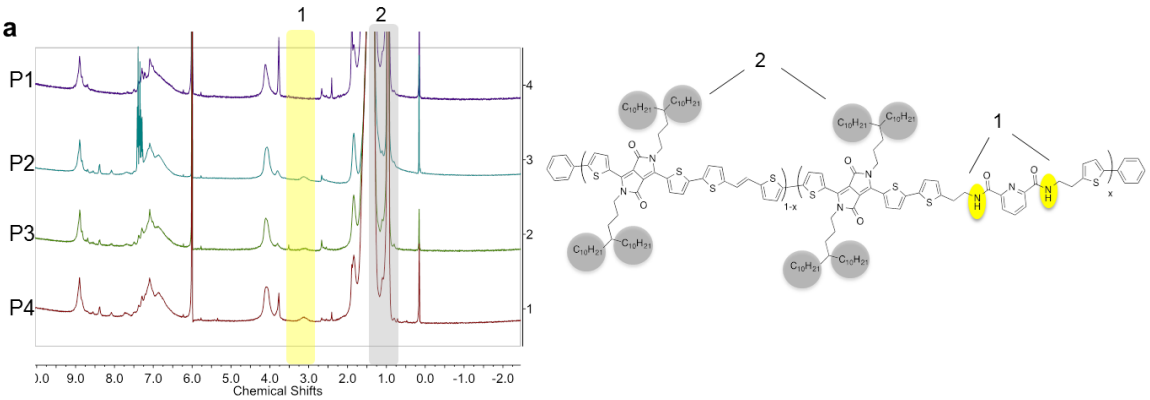

b

	Theoretical ratio (1:2)	Calculated ratio (1:2)	M_n (kDa)	M_w (kDa)	PDI	T_d[a]	λ_{max} Sol,(nm)	λ_{max} Film,(nm)	HOMO[b] (eV)	Bandgap[c] (eV)
P1	0.00	0.00	20.4	65.4	3.2	>350	803, 738	801, 740	5.17	1.35
P2	0.05	0.06	19.7	61.4	3.3	>350	803, 738	801, 739	5.22	1.35
P3	0.10	0.09	16.2	49.1	3.0	>350	803, 738	801, 738	5.23	1.35
P4	0.20	0.17	13.4	35.5	2.6	>350	803, 738	801, 734	5.17	1.37

Extended Data Figure 1 | General characterization of P1-P4. a) Polymer composition by ^{1}H NMR. The ratio of PDCA moieties incorporated in the polymer backbone is determined by the integration of amide protons (**1**) vs the alkyl chains terminal protons (**2**); b) General characterization of **P1**-**P4**.

[a] Determined from thermogravimetric analysis (TGA).

[b] The HOMO energy level was calculated from cyclic voltammetry. Potentials Vs Ag/AgCl using 0.1 M $TBAPF_6$ in CH_3CN as electrolyte.

[c] Calculated by the following equation: gap = $1240/\lambda_{onset}$ of polymer film.

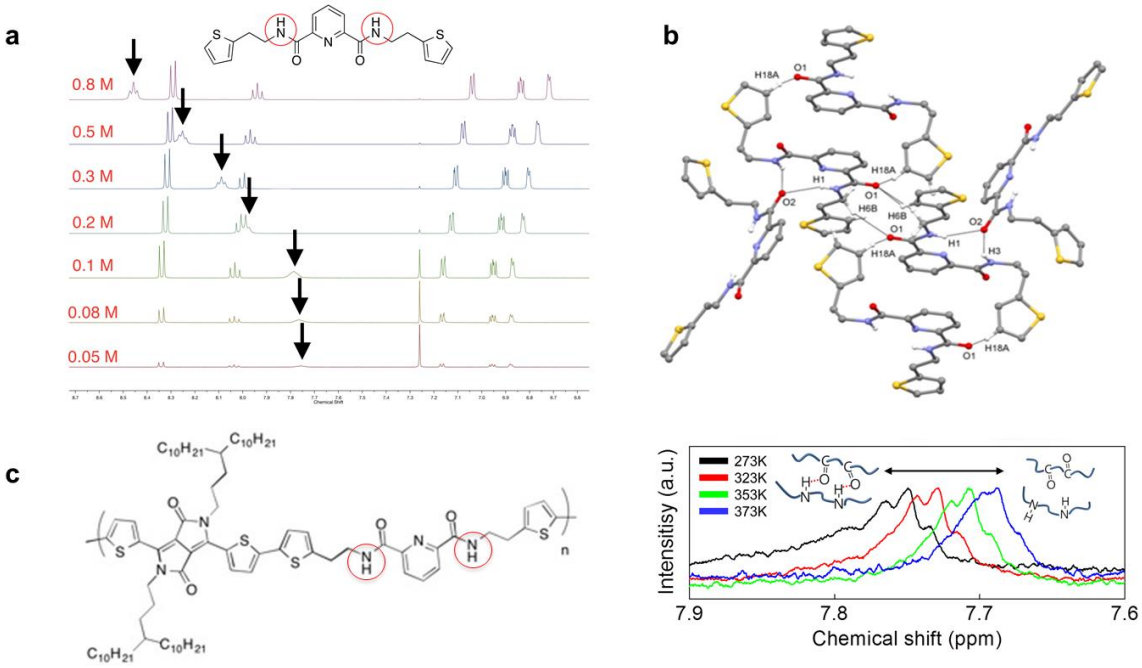

Extended Data Figure 2 | Intermolecular interactions between 2,6-pyridine dicarboxamide (PDCA) moieties. a) Chemical structure of model compound **1** and ^{1}H NMR at various concentration of compound **1** in $CDCl_3$. Upon increasing concentration from 0.05 M to 0.8 M, a distinct shift of the amide proton (black arrow) towards low fields is observed. This indicates formation of hydrogen bonding between the PDCA moieties similar as previous report (see reference 38 in Supplementary Information). A dimerization constant of 0.18 M^{-1} was determined by plotting concentration vs chemical shift and fitting using dimer association model (see reference 44 in Supplementary Information); b) Molecular structure of **1** showing intermolecular hydrogen bonds determined by single crystal X-rays diffraction. Ellipsoids are set at 30% probability level. Selected hydrogen atoms are omitted for clarity; c) Chemical structure of model oligomer **M1** and ^{1}H NMR of **M1** at various temperature in 1,1,2,2-tetrachloroethane-d_2 (zoomed on amide peak). The chemical shift upon temperature increase indicates a breaking of the hydrogen bonds formed between the polymer chains. Oligomer **M1** was used for this study because the solubility of the polymer was not sufficiently high to perform a similar study under high concentrations.

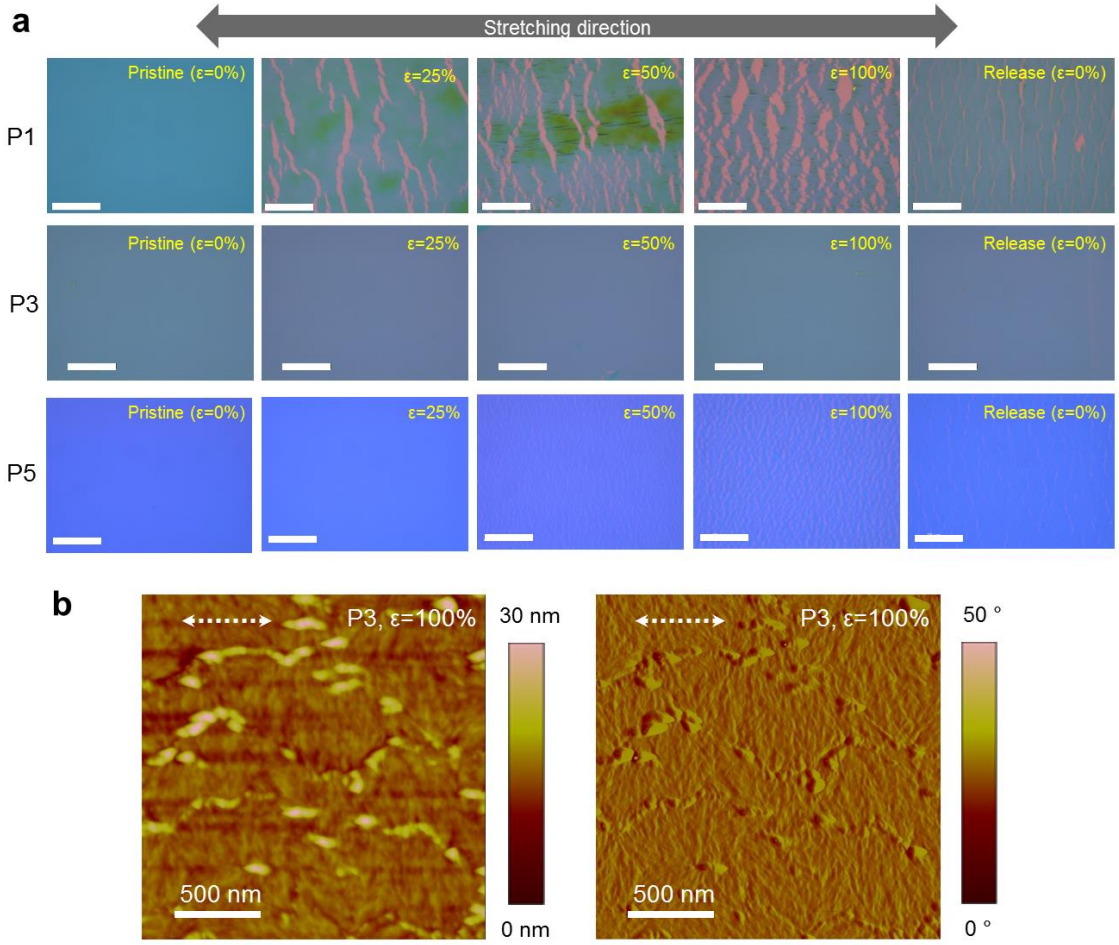

c

Polymer	Applied Strain	FWHM at (200) peak <parallel>	Mean size of crystallites (nm)	FWHM at (200) peak <perpendicular>	Mean size of crystallites (nm)
P1	ε = 0%	0.0422	13.8	0.0417	14.0
	ε = 50%	0.0461	12.7	0.0489	11.9
	ε = 100%	0.0517	11.3	0.0554	10.5
	Release	0.0502	11.6	0.0525	11.1
P3	ε = 0%	0.0497	11.8	0.0494	11.8
	ε = 50%	0.0527	11.1	0.0526	11.1
	ε = 100%	0.0503	11.6	0.0524	11.2
	Release	0.0493	11.8	0.0491	11.9

Extended Data Figure 3 | Behavior of polymer thin film under strain. a) Optical microscope images of **P1**, **P3**, and **P5** as function of applied strains (0-100%). b) Height and phase AFM images of **P3** under 100% strain showing no crack formation. c) Table of grazing-incident XRD data for **P1** and **P3** films as a function of strains (0-100%). The samples are annealed at 150°C for 10 min. A reduction in the mean size of crystallites is observed for **P1** to **P3**.

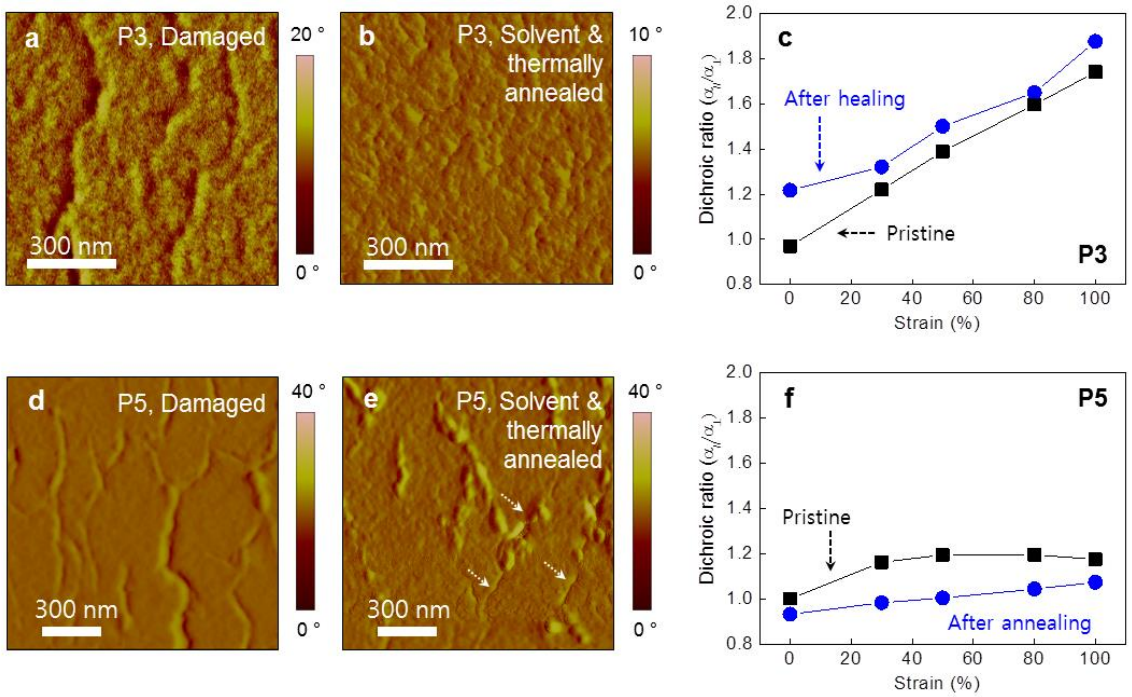

Extended Data Figure 4 | Thin films characterization of damaged and healed P3 and P5. Atomic force microscopy images of a) damaged and b) healed thin film of **P3** after solvent and thermal annealing. We note that all the previously observed nanocracks were absence after the healing process; c) dichroic ratio of **P3** healed thin film as determined by polarized UV-vis spectroscopy; Atomic force microscopy images of d) damaged and e) solvent and thermally annealed thin film of **P5.** We observed that a small number of nanocracks remained in the film; c) dichroic ratio of **P5** healed thin film determined by polarized UV-vis spectroscopy. It was observed that the dichroic ratio of healed film of **P3** fully recovered to a value similar as the pristine film without damage. On the other hand, when **P5** is subjected to the same treatment, the dichroic ratio was not restored, indicating that the movement of the polymer chains was insufficient to restore the film's mechanical properties.

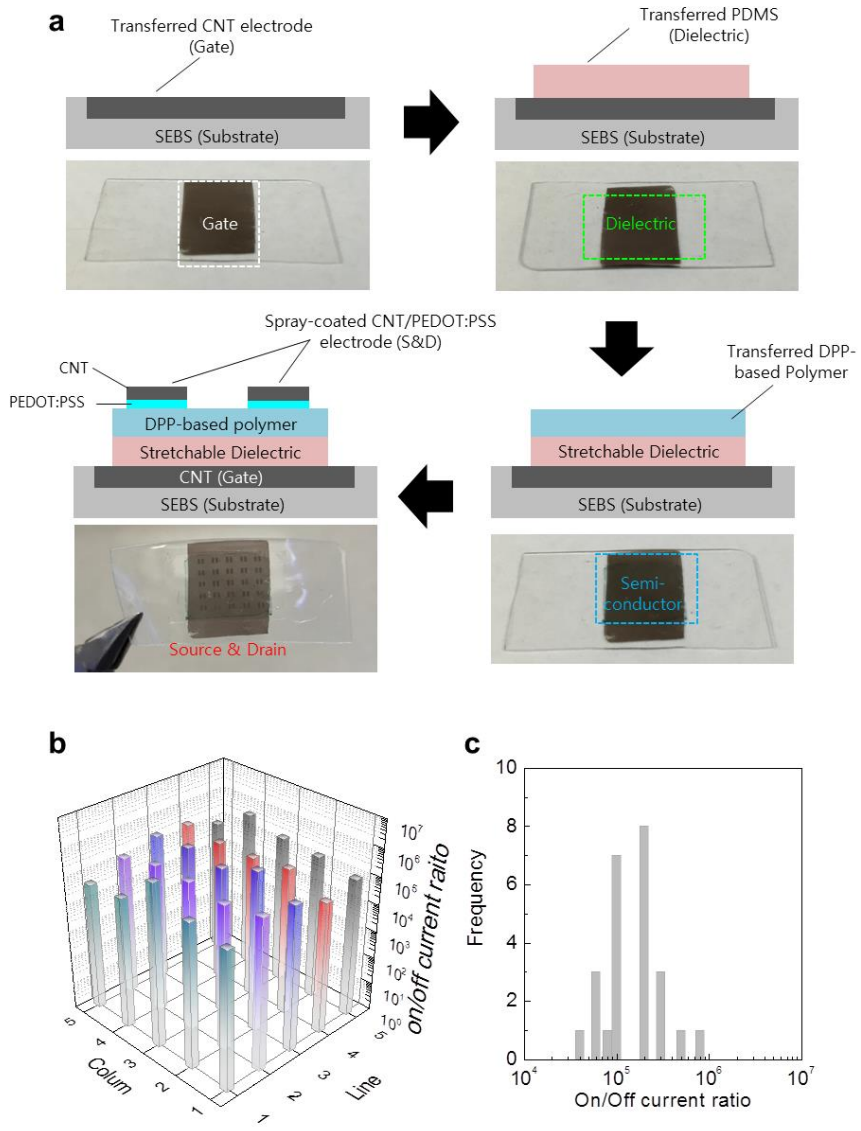

Extended Data Figure 5 | Fabrication and electronic properties of a fully stretchable 5x5 transistor array. a) Fabrication process of fully stretchable OTFTs: 1) Transfer printing of CNT gate electrode as prepared by spray coating a CNT solution (10 mg/ml in $CHCl_3$) on SEBS substrate (Thickness: 200 μm). 2) Contact transfer printing of PDMS dielectric layer as prepared by a spin coating a diluted PDMS (220 mg/ml in $CHCl_3$) on OTS-treated SiO_2 substrate on CNT gate electrode. 3) Contact transfer printing of semiconducting polymer layer (prepared by spin coating on OTS-treated SiO_2 substrate) on PDMS dielectric layer. 4) Spray coating of CNT (70 nm)/PEDOT:PSS (30 nm) source and drain electrodes on semiconducting layer. b) on/off current mapping and c) statistical distribution of 5x5 fully stretchable OTFT arrays (Width: 1000 μm, Length: 150 μm).